Ultrafast and High Extinction Ratio 1×4 Electro-Optical Switch Based on Cascaded Dual-Output MZI

Zhiyong Wang, Meihua Xiang, Feng Yang, Kunlun Liu, Jianfeng Bao, Dengcai Yang, and Yunxin Wang

***Abstract*—We propose and fabricate an ultrafast and high extinction ratio 1 × 4 optical switch based on a cascade, dual-output Mach–Zehnder interferometer (MZI) on the lithium niobate platform. The optical switch consists of cascaded, identical, dual-output MZI structures, and each of them includes a Y-branch waveguide, two parallel interference arms (electrode action area), and a 3 dB directional coupler. Four output optical paths can be switched through three groups of electrode hierarchical modulation. The test results of the fabricated device show that the insertion loss of each port is less than 7.1 dB and that the maximum extinction ratio is higher than 39.3 dB. The optical switch can achieve a high extinction ratio greater than 20 dB within the 50 nm wavelength range. The measured half-wave voltage is less than 4.13 V, and the minimum switching rise and fall times reach 125 ps and 250 ps, respectively. This result shows that the proposed and fabricated 1 × 4 integrated optical switch on a lithium niobate platform has the advantages of a fast response rate, high extinction ratio, and low switching voltage.**

***Index Terms*—1 × 4 electro-optical switch, dual-output MZI, optical waveguide, ultrafast and high extinction ratio.**

I. Introduction

OPTICAL switches have displayed many advantages, such as high speed, transparency, and low power consumption, in all-optical internet applications and have been widely employed in optical communication packet switching [1], optical computing [2], and quantum key distribution [3]. With the increasing requirements for communication quality and speed, higher requirements are proposed for the extinction ratio [4], [5], switching speed [6], multiple ports [7], and insertion loss [8] of optical switches. Microelectromechanical system (MEMS) optical switching is relatively mature and can be employed for large array network architecture with good extinction ratio performance but limited speed (∼ms) [9], [10], [11]. Waveguide optical switching uses the electro-optic effect, acousto-optic effect, and thermo-optic effect to realize the optical switch function. The electro-optic switch has the fastest response speed (∼ns) and low heat, which is suitable for small signal optical communication [12], [13]. Waveguide optical switches composed of various Planar Lightwave Circuits (PLCs) are the most attractive switching devices. Because of their reliability, flexibility, and ease of integration, PLCs can be utilized in wavelength division multiplexing (WDM) optical fiber communication systems to achieve optical cross-connection and optical add-drop multiplexing [14], [15]. These types include the Y-junction [16], X-junction [17], directional coupler (DC) [18], [19], [20], [21], ring [22], [23], resonant ring (MRR) [13], [24], multimode interferometer (MMI) [25], [26], and Mach–Zehnder interferometer (MZI) [27], [28]

The conventional MRR electro-optical switch unit has a small volume and high process requirements and is generally used to realize multiwavelength matrix optical switches. Both the switch unit of the 2 × 2 multiwavelength, silicon-based optical switch with an MRR structure [13] and the cross-matrix, silicon-based optical switch with an MRR structure [24], which showed good scalability but poor extinction performance (∼20 dB), have been proposed. An expandable 2 × 2 MMI structure optical switch based on silicon [26], which has a large tolerance and compact structure for dense wavelength division multiplexing systems, has also been developed. The MZI optical switch based on the directional coupler has good extinction performance but a large interference structure size, which is generally utilized to make 1 × 2 and 2 × 2 light switch structures. Because the reverse cone can increase the operating wavelength bandwidth, a reverse cone directional coupling structure 2 × 2 MZI lithium niobate optical switch [29], which has a switching time of 30 ns, a switching voltage of 6 V, and an extinction ratio of 35 dB, has been proposed. While multiple MZI building blocks are cascaded into arrays, multiport optical switching devices can be composed. Therefore, 1 × 4 and 1 × N directional coupling structures of lithium niobate, MZI optical switches [30], [31] have been proposed and simulated, respectively. However, neither of them has fabricated the devices nor conducted actual experimental

Manuscript received 9 February 2023; revised 31 March 2023; accepted 11 April 2023. Date of publication 13 April 2023; date of current version 26 April 2023. This work was supported by the National Natural Science Foundation of China under Grants 61871007 and 62275008. *(Corresponding author: Feng Yang.)*

Zhiyong Wang, Meihua Xiang, Kunlun Liu, Jianfeng Bao, and Dengcai Yang are with the Institute of Laser Engineering, Faculty of Materials and Manufacturing, Beijing University of Technology, Beijing 100124, China, and also with the Institute of Advanced Technology on Semiconductor Optics & Electronics, Beijing University of Technology, Beijing 100124, China (e-mail: zywang@bjut.edu.cn; xiangmh@emails.bjut.edu.cn; liukunlun2021@126.com; baojf@emails.bjut.edu.cn; dengcaiyang@bjut.edu.cn).

Feng Yang and Yunxin Wang are with the College of Physics and Optoelectronics, Faculty of Science, Beijing University of Technology, Beijing 100124, China, and also with the Beijing Engineering Research Center of Precision Measurement Technology and Instruments, Beijing University of Technology, Beijing 100124, China (e-mail: fengyang@bjut.edu.cn; yxwang@bjut.edu.cn).

Digital Object Identifier 10.1109/JPHOT.2023.3266953

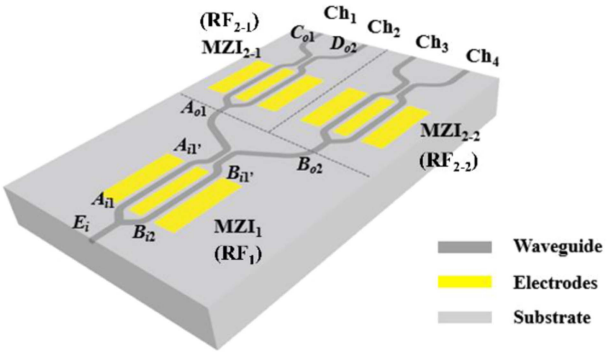

Fig. 1. Schematic of the 1 × 4 optical switch.

tests. A 1 × 2 YBB-MZI structure lithium niobate modulator has been proposed and used as an electric field sensor [32]. The MZI structure contains a directional coupler that can serve as an optical switch with a switching voltage of approximately 16.6 V and an extinction ratio of 14.7 dB.

In this paper, a novel ultrafast and high extinction ratio 1 × 4 optical switch on the lithium niobate platform is proposed and fabricated. The optical switch consists of identical, cascaded, dual-output MZI structures, each of which includes a Y-branch waveguide, two parallel interference arms (electrode action area), and a 3 dB directional coupler. The Y-branch waveguide has the advantages of a wide operating wavelength and large process tolerance, and the electrode in parallel interference arms adopts a push-pull, traveling wave electrode structure, which can realize broadband modulation. The 3 dB directional coupler is beneficial for improving the extinction ratio of the switching. All can fully utilize their advantages in the designed array optical switch. Four output optical paths can be switched through three groups of electrode hierarchical modulation. The influence of the coupling distance and coupling length of the directional coupler on the wavelength bandwidth and process tolerance is analyzed, and the optimized parameters of the MZI optical switch unit are obtained. The test results show that the insertion loss of the four ports is less than 7.1 dB, the maximum extinction ratio is higher than 39.3 dB, and a high extinction ratio greater than 20 dB in the wavelength range of 50 nm can be achieved. The measured half-wave voltages are less than 4.13 V, and the minimum switching rise and fall times reach 125 ps and 250 ps, respectively. The experimental results show that the proposed and fabricated 1 × 4 integrated optical switch has the advantages of a fast response rate, high extinction ratio, and low switching voltage.

II. Device Structure and Theoretical Analysis

Fig. 1 shows a schematic of the proposed 1 × 4 electro-optical switch, which consists of identical, cascaded, dual-output MZI structures. Each dual-output MZI includes a Y-branch waveguide, two parallel interference arms (electrode action area), and a directional coupler. The two outputs of the directional coupler are complementary and can be controlled by the driving voltage difference of the parallel interference arm. After the two outputs of the first-stage, dual-output MZI, each followed the same dual-output MZI, and then the 4-outputs can be achieved.

Assume that the input lightwave can be expressed as $E_{\text{in}}(\text{t}) = E_0 e^{j\omega t}$, where E_0 and ω are its amplitude and angular frequency, respectively. The lightwave passes through the Y branch and is then divided into two parts, which are written as

$$A_{i1} = B_{i2} = \frac{E_0}{\sqrt{2}} e^{j\omega t} \tag{1}$$

A driving voltage is applied to the two parallel interference arms through the modulated electrodes to change the waveguide refractive index. The phase difference of the optical signal between the two arms caused by the driving voltage is

$$\varphi_1 = \frac{2\pi}{\lambda} \Delta n_e L = -\frac{\pi}{\lambda} n_e^3 \gamma_{33} E_z \Gamma L \tag{2}$$

where λ is the wavelength of the input lightwave, γ_{33} is the electro-optical coefficient of lithium niobate (∼30.8 pm/V), n_e is the refractive index of extraordinary waves, L is the electrode length, Γ is the overlap integral of the light field passing through the electrode area and electric field, and E_z is the electric field intensity. When the electrode adopts a push-pull structure, the output lightwave of the upper and lower arms after being modulated by the driving voltage is expressed as

$$\begin{pmatrix} A_{i1'} \\ B_{i2'} \end{pmatrix} = e^{j\omega t} \begin{pmatrix} e^{j\varphi_1/2} & 0 \\ 0 & e^{-j\varphi_1/2} \end{pmatrix} \begin{pmatrix} A_{i1} \\ B_{i2} \end{pmatrix} \tag{3}$$

where $A_{i1'}$ and $B_{i2'}$ are the outputs of two parallel interference arms, A_{i1} and B_{i2} are the outputs of the Y-branch.

A directional coupler follows the parallel interference arms, and the outputs of the two ports are

$$\begin{pmatrix} A_{o1} \\ B_{o2} \end{pmatrix} = e^{j\omega t + j\beta L_{c1}} \begin{pmatrix} \cos\kappa_1 L_{c1} & -j\sin\kappa_1 L_{c1} \\ -j\sin\kappa_1 L_{c1} & \cos\kappa_1 L_{c1} \end{pmatrix} \begin{pmatrix} A_{i1'} \\ B_{i2'} \end{pmatrix} \tag{4}$$

where A_{o1} and B_{o2} are the outputs of the directional coupler, β is the number of lightwaves, κ_1 and L_{c1} are the coupling coefficient and coupling length, respectively, of the first-stage directional coupler.

Since the MZI structures in the two stages have the same structure, the two stage MZI structures have the same transfer functions. Then, the 4-outputs of the 1 × 4 optical switch are expressed as

$$\begin{cases} P_1 = \frac{|E_0|^2}{4} [1 + \sin(2\kappa_1 L_{c1}) \sin\varphi_1] \\ \qquad [1 + \sin(2\kappa_2 L_{c2}) \sin\varphi_2] \\ P_2 = \frac{|E_0|^2}{4} [1 + \sin(2\kappa_1 L_{c1}) \sin\varphi_1] \\ \qquad [1 - \sin(2\kappa_2 L_{c2}) \sin\varphi_2] \end{cases} \tag{5}$$

$$\begin{cases} P_3 = \frac{|E_0|^2}{4} [1 - \sin(2\kappa_1 L_{c1}) \sin\varphi_1] \\ \qquad [1 + \sin(2\kappa_3 L_{c3}) \sin\varphi_3] \\ P_4 = \frac{|E_0|^2}{4} [1 - \sin(2\kappa_1 L_{c1}) \sin\varphi_1] \\ \qquad [1 - \sin(2\kappa_3 L_{c3}) \sin\varphi_3] \end{cases} \tag{6}$$

TABLE I
SWITCHING STATUS OF THE 4 OUTPUTS BY THE DRIVING VOLTAGE OF THE CASCADED MZI

RF_1	$RF_{2\text{-}1}$	$RF_{2\text{-}2}$	CH_1**	CH_2**	CH_3**	CH_4**
V_π	V_π	--	1	0	0	0
	0	--	0	1	0	0
0	--*	V_π	0	0	1	0
	--	0	0	0	0	1

* Driving voltage status: 0—low level, V_π—high level, and -- — any state.
** Switching status of the 4-outputs: 0 — off and 1 — on.

where κ_2 and κ_3 are the coupling coefficients, L_{c2} and L_{c3} are the coupling lengths of the second-stage directional coupler, φ_2 and φ_3 are the phase differences between the two arms of MZI_{2-1} and those of MZI_{2-2}, respectively.

To maximize the extinction ratio of the optical switch, the coupling length of the directional coupler in the two stages shall meet

$$\begin{cases} \sin(2\kappa_1 L_{c1}) = 1 \\ \sin(2\kappa_2 L_{c2}) = 1 \\ \sin(2\kappa_3 L_{c3}) = 1 \end{cases} \tag{7}$$

that is, $\kappa_1 \quad L_{c1} = \kappa_2 \quad L_{c2} = \kappa_3 \quad L_{c3} = \frac{(2n+1)\pi}{4}$, $(n = 0, 1, 2, \ldots)$. Therefore, the two-stage directional couplers shall be designed as 3 dB directional couplers.

When the phase difference of the electro-optical between the upper arm and the lower is $+\pi/2$ or $-\pi/2$, the power of the two outputs of the MZI can achieve the maximum or minimum, respectively. That is, the output of the MZI can be switched by the voltage difference between the two parallel interference arms, and the switching voltage is the voltage difference with the phase change π between the upper arms and the lower arms, which is also referred to as the half-wave voltage (V_π) of the modulator. The proposed 1×4 $LiNbO_3$ electro-optical switch adopts a cascaded MZI array. While the upper output port of the first-stage MZI reaches the maximum output by controlling the voltage, the CH_1 and CH_2 outputs can be controlled by the control voltage of MZI_{2-1}. Similarly, when the lower output port of the first-stage MZI reaches the maximum output, the CH_3 and CH_4 outputs can be controlled by the control voltage of MZI_{2-2}. The switching states of the 4-outputs by the driving voltage of the cascaded MZI in the proposed 1×4 optical switch are shown in Table I.

III. DESIGN AND FABRICATION

The dual-output MZI is composed of a Y-branch waveguide, two parallel interference arms, and a directional coupler, and the directional coupler is the key part of the proposed 1×4 electro-optical switch. According to (7), to achieve a high extinction ratio of the electro-optical switch, the directional coupler should be designed as a 3 dB directional coupler. The substrate of the proposed electro-optical switch is constructed of x-cut lithium niobate material, and the waveguide core layer is formed by annealing proton exchange (APE) on the substrate. The structure of the 3 dB directional coupler is shown in Fig. 2. According to the size of the electrode spacing, the spacing (h1) between the input waveguides can be set to 23 μm. The spacing of the coupling fiber at the output ports is 127 μm, so the spacing (h2) between the two adjacent output waveguides should be 254 μm. The size of the single-mode waveguide is 6.5 μm, and the curved waveguide type is a cosine function shape (Cos-S). To ensure the transmission performance and minimize the size requirement, La1 and Lb1 are set to 2000 μm and 8000 μm, respectively, in the bend section.

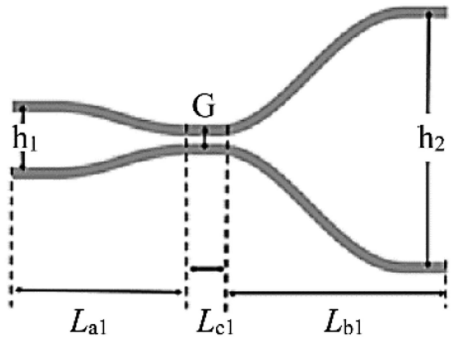

Fig. 2. Structure of the directional coupler.

TABLE II
OPTIMAL COUPLING LENGTH (L_{c1}) WITH DIFFERENT COUPLING SPACINGS (G)

Number	G (μm)	L_{c1} (μm)
1	8	635
2	9	1435
3	10	262
4	11	870
5	12	1850

In the coupling area of the directional coupler, as shown in Fig. 2, different coupling spacings (G) should match the specific optimal coupling lengths (Lc1). The optical field transmission of the directional coupler is simulated by the OptiBPM. Setting the coupling spacing to 8 μm, 9 μm, 10 μm, 11 μm and 12 μm, the minimum coupling length for different coupling distances was obtained under the condition of ensuring a 50:50 equal beam splitting by monitoring the optical power ratio between the two outputs, as shown in Table II.

When the coupling spacing is small, the coupling effect between the curved waveguide segments of the directional coupler will be enhanced, and there will be coupling between the falling and rising waveguide segments of the input and output, and the superposition with the parallel main coupling regions will form a secondary overlapping coupling phenomenon. In order to obtain an exactly beam splitting ratio of 50:50, the selected optimal coupling region length should be increased. As the coupling distance increases, the coupling effect between the curved waveguide segments of the directional coupler will decrease, and the main coupling effect will be in the parallel coupling region. Therefore,

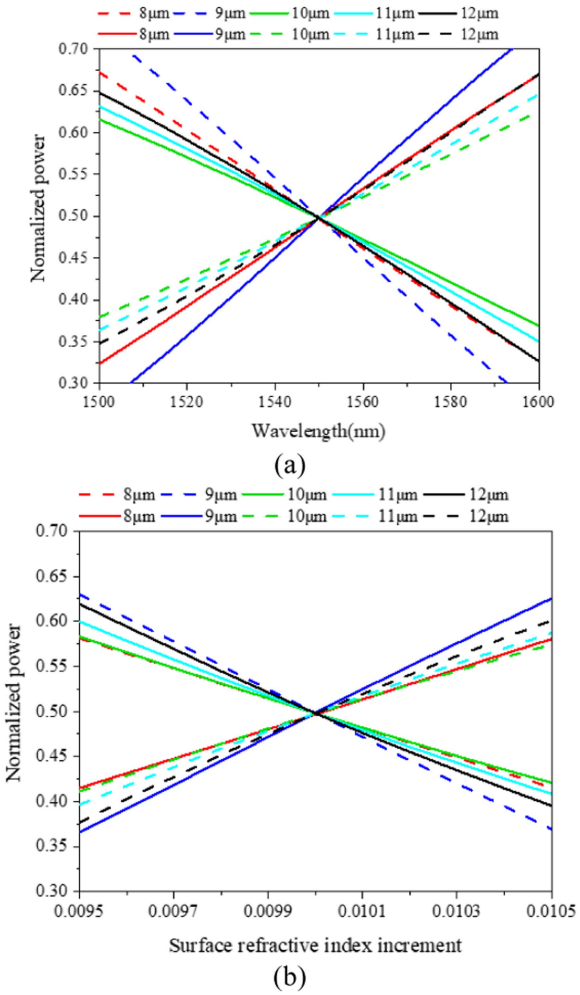

Fig. 3. Simulated normalized output power of two ports of the directional coupler in simulation, (a) with different operating wavelengths and (b) with different surface refractive index increments.

there is only one overlapping coupling, and the optimal coupling region length will increase with the coupling distance. As shown in Table II, when the spacing is less than 10 μm, the influence of the optimal coupling length on the curved waveguide portion is not monotonic, while it is greater than or equal to 10 um, the change of it is monotonic.

In addition, different coupling distances will affect the wavelength bandwidth characteristics of the directional coupler. To achieve a high extinction ratio electro-optical switch with a large spectral bandwidth, the directional coupler should be as insensitive to the wavelength as possible and have a spectroscopic ratio of nearly 50:50 over a wide wavelength range. To investigate the operating wavelength range of the directional couplers with different coupling spacings, a simulation was performed; the results are shown in Fig. 3(a). The solid and dashed lines represent the normalized output power of the two output ports. When the central wavelength is 1550 nm, an equal power distribution between the two ports can be achieved. However, due to the influence of waveguide dispersion, the power consistency of the output port worsens when the wavelength deviates from the central wavelength. The results show that when the coupling

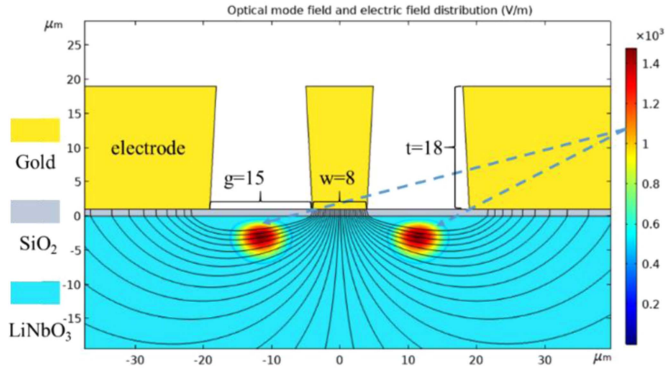

Fig. 4. Electric and mode field distribution of the CPW electrode.

spacing is 10 μm, the coupling efficiency of the two ports changes more slowly with wavelength.

In the process of waveguide fabrication, process defects lead to refractive index deviation in the waveguide region. To analyze the refractive index tolerance of directional couplers with different coupling spacings, the output characteristics of two ports with different coupling spacings and different refractive index differences are simulated and analyzed. The simulation results are shown in Fig. 3(b), where the increment of the surface refractive index is the refractive index difference between the surface of the APE lithium niobate crystal and the substrate. The normalized output power of the two ports changes slowly with increasing surface refractive index, that is, it is insensitive to refractive index changes and has a larger tolerance.

According to the above simulation and analysis, taking into account factors such as process error, waveguide dispersion, and the loss caused by waveguide length, the coupling spacing is set to 10 μm, and the corresponding coupling length is 262 μm. With the same method, by simulating the ideal field transmission paths with different coupling region lengths, the optimal coupling length for both Lc2 and Lc3 of MZI_{2-1} and MZI_{2-2} is 378 μm. To take into account the switching voltage and transmission loss of the device, the length of the interference arms is set to 2 cm, so the total length of the device is 7 cm.

Furthermore, the electrode parameters of the electro-optical switch are designed. A push-pull coplanar waveguide (CPW) traveling wave electrode structure, which can obtain a smaller switching voltage and larger modulation bandwidth, has been adopted and is the key to ensuring the high-frequency characteristics of electro-optical switches. The simulation of the traveling wave electrode structure of a doped lithium niobate substrate based on the finite element method with COMSOL has been performed. The model of the electrode cross-section is shown in Fig. 4. The electrode length, width, and thickness are 2 cm, 8 μm, and 18 μm, respectively, where the black curve represents the electric field distribution near the waveguide and the irregular circular spot represents the optical mode field distribution in the waveguide. By analyzing the influence of electrode structure parameters on the microwave effective refractive index, characteristic impedance, and other characteristic parameters, the electrode structure parameters can be optimally designed; all

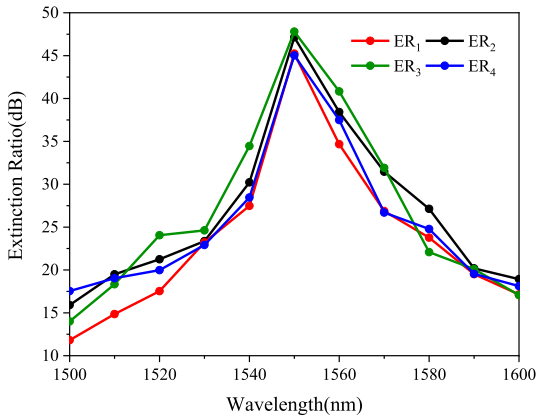

Fig. 5. Simulated switching extinction ratio of the optical switch at different wavelengths.

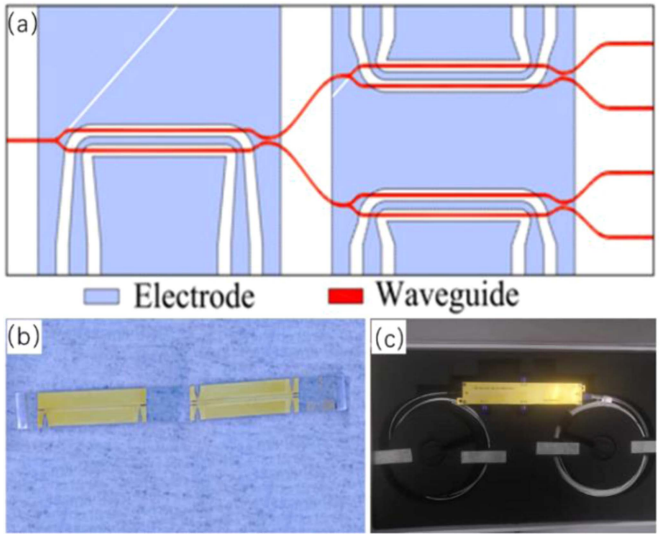

Fig. 6. (a) Process layout, (b) optical switch chip, and (c) packaged device of the 1 × 4 electro-optical switch.

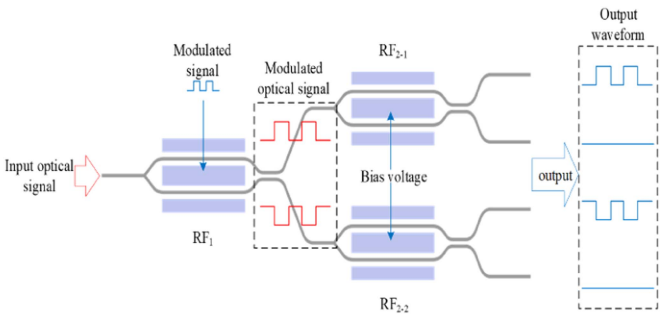

Fig. 7. Experimental schematic for the 1 × 4 electro-optical switch.

are marked in Fig. 4. The electro-optical overlap integral, the characteristic impedance of the electrode (@ 10 GHz) and the effective refractive index of the microwave are 0.52, 37 Ω and 2.12, respectively, the phase velocity and impedance are well matched.

The performance of the extinction ratio with different wavelengths has been simulated by OptiBPM. By controlling the three electrodes, the four output ports are switched. The extinction ratio of the four ports at different wavelengths is shown in Fig. 5. The results show that the extinction ratio of the four ports at 1550 nm is greater than 45 dB. A switching extinction ratio greater than 20 dB can be achieved in the wavelength range of 1530 nm ∼ 1580 nm.

Then, we followed the design parameters for the electro-optical switch and fabricated the device. Optical waveguides were fabricated on an x-cut lithium niobate substrate by APE [33]. The lightwave propagates along the y-direction of the crystal with a waveguide width of 6.5 μm and works in TE mode. The benzoic acid solution diluted with lithium benzoate was proton exchanged for 4 hours and then annealed for 6 hours to obtain a waveguide for single-mode operation. A gold electrode with a thickness of 18 μm is fabricated by secondary lithography and electroplating. After cutting, the end face of the chip is processed to an inclination angle of 10° by a chemical mechanical polishing process, and an optical fiber array with a corresponding inclination angle of 15° is coupled with it, which is conducive to reducing back reflection. The polished lithium niobate end-face and the optical fiber end-face are precisely aligned and coupled by a 6-dimensional regulating frame platform. In addition, the standard V-slot with a spacing of 127 μm is employed for the output optical fiber array, which is similar to the coupling technology of PLC and can achieve good channel insertion loss consistency. The device was packaged in a shell that was constructed of Kovar material.

The layout of the proposed device is shown in Fig. 6(a), and the electro-optical switch chip after the fabrication of the waveguide and electrode is shown in Fig. 6(b). The coupled device is fixed in a metal shell using silicone rubber, and the electrodes and metal pins are bonded with gold wires. The encapsulated 1 × 4 electro-optical switch is shown in Fig. 6(c). The electro-optical switch device has a length of 70 mm and a width of 17 mm.

IV. Device Measurement and Discussion

The performance of the fabricated electro-optical switch is performed, the insertion loss and extinction ratio with different operating wavelengths are tested, and a schematic of the experimental setup is shown in Fig. 7. A wavelength- switchable light source with a spectrum range of 1520 nm∼1580 nm is injected into the electro-optical switch. Three DC voltage sources are employed to set the switching status. The configuration of the 1 × 4 electro-optical switch is shown in Table I. The driving voltage of the electro-optical switch is controlled to maximize the output power of the corresponding output port. An optical power meter is used to measure the maximum power of the corresponding port. The difference between the measured power and the input power is the insertion loss. Changing the wavelength of the input light, the insertion loss with different wavelengths is tested; the test results are shown in Fig. 8. The black, red, green, and blue dots correspond to the insertion loss of ports 1, 2, 3, and 4, respectively. The insertion loss at 1550 nm reaches minima of 6.77 dB, 6.96 dB, 6.75 dB, and 7.1 dB for the corresponding

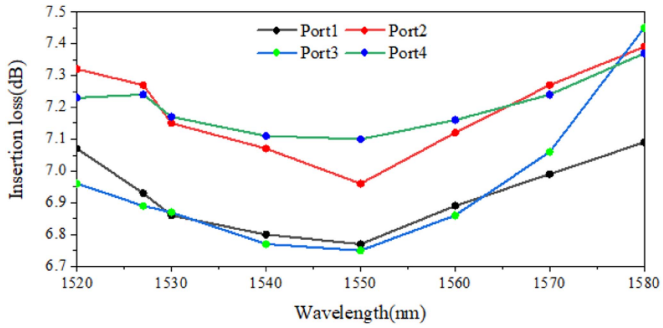

Fig. 8. Tested insertion loss with different wavelengths.

ports. The insertion loss increases with the wavelength far from 1550 nm mainly because the power consistency of the output port of the directional coupler worsens as it deviates from the center wavelength. This declining consistency is caused by waveguide dispersion and refractive index deviation by process defects, which is consistent with the simulation results in Fig. 3.

The switching voltage of the electro-optical switch is a very important parameter, that is, the half-wave voltage of the MZI. This is the voltage difference when the best extinction ratio is achieved in the on/off state; it determines the driving power of the electro-optical switch. In the experiment, the triangle waveform driving signal is utilized as the half-wave voltage test of the electro-optic switch.

Light with a wavelength of 1550 nm is input into the electro-optical switch. The signal generator loads a triangle wave signal with a frequency of 1 kHz into one RF port of the electro-optical switch. While setting the other RF ports to the ON state and ensuring that the corresponding port outputs the maximum power, the output waveform of the electro-optical switch can be displayed on the oscilloscope after detection by a photodetector. The amplitude of the triangle wave signal output by the signal generator is adjusted, so that the output signal of the electro-optical switch displays a sine wave on the oscilloscope for at least one complete cycle. The same method was used to test all RF ports as above; all the results are shown in Fig. 9. According to the test results and calculation, the half-wave voltages of the three electrodes are 4.13 V, 3.46 V, and 3.61 V. The test results are slightly larger than the simulation result of 3.5 V, and there are some differences between them, which are attributed to the error of the electrode process in the actual process.

Then, the switching extinction ratio of the electro-optical switch is also analyzed. Using the experimental schematic shown in Fig. 7, setting the driving voltage of the RF port according to the configuration shown in Table I and the half-wave voltage results shown in Fig. 9, an optical power meter is used to test the optical power difference between the ON state and OFF state for each channel, which is the switching extinction ratio. The wavelength of the tunable light source is changed, and the switching extinction ratio is tested at different wavelengths for each channel. The test results are shown in Fig. 10. The maximum extinction ratios of the four output ports are 39.68 dB, 41.54 dB, 43.45 dB, and 39.50 dB. With the exception of CH_4, the extinction ratio of the other three ports reaches a maximum

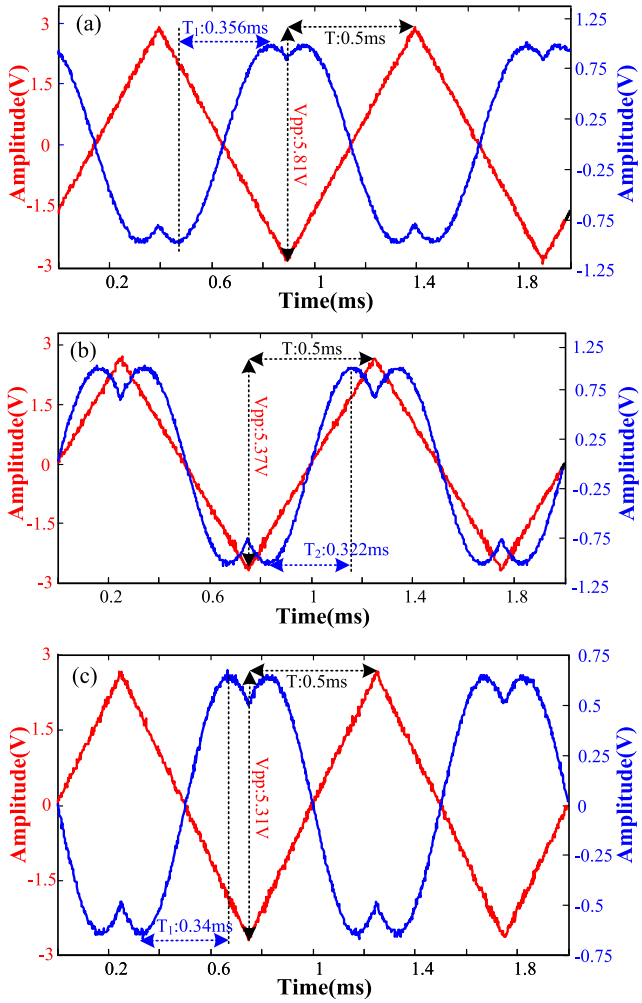

Fig. 9. (a), (b) and (c) are the half-wave voltage test results of the first, second, and third groups of electrodes, respectively.

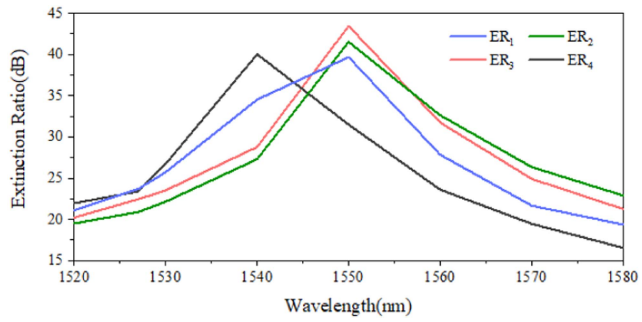

Fig. 10. Extinction ratio of the electro-optical switch at different wavelengths.

at the central wavelength of 1550 nm. For all 4 ports, a 20 dB extinction ratio bandwidth of 50 nm is achieved. The deviation in the maximum extinction ratio of the 4 ports from the central wavelength is mainly caused by the manufacturing process error.

The switching response of the fabricated electro-optical switch is tested. A 1550.12 nm continuous laser (NKT, Koheras BASIK X15) is connected to the electro-optical switch. An arbitrary waveform generator (AWG, Tektronix AWG70002B)

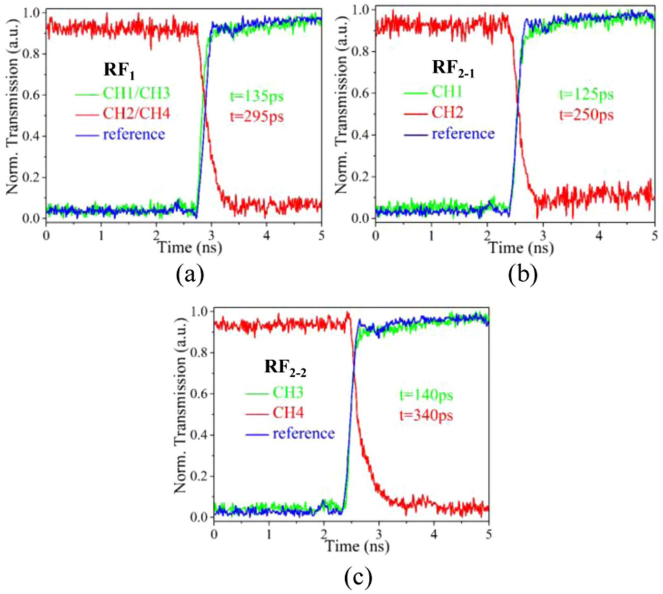

Fig. 11. (a), (b), and (c) show the rise and fall times of the three RF ports with pulse driving voltage.

followed by a high-speed voltage amplifier (Conquer, KG-EOD-10G) is selected as the pulse voltage source, which is combined with a DC voltage through a Bias-TEE and then injected into the RF port of the electro-optical switch. The optical signal was detected by a photodetector (Conquer, KG-PD-20G, 20 GHz, 0.75 A/W), and an oscilloscope (Tektronix DPO75902SX) is employed to monitor the response waveforms.

According to the configuration of the switching status in Table I, the pulse signal is loaded into the RF_1 port, and the RF_{2-1} port is configured at a high level so that only the CH_1 port can detect the forward pulse signal. When testing the RF_{2-1}port with a pulse signal, the RF_1 port should be configured with a high level. Similarly, when testing RF_{2-2}, the RF_1 port should be configured with a low level. When RF_{2-1} and RF_{2-2} are loaded with the pulse signal test, the switch statuses of CH_1 and CH_2, CH_3 and CH_4 are opposite, respectively.

Fig. 11 shows the output waveform when the RF port of the optical switch is loaded with high-speed pulse signals at the RF drive ports, where the blue curve is the reference waveform of the driving signal loaded into the RF port. When the RF_1 port is loaded with a pulse driving signal, the rising edge signal will be observed at the CH_1 or CH_2 port, and the falling edge signal will be observed at the CH_3 or CH_4 port, where the output of CH_1 or CH_2 also needs to be controlled by the driving voltage state of the RF_{2-1} port, and CH_3 or CH_4 is controlled by the driving voltage state of the RF_{2-2} port. As shown in Fig. 11(a), the rise time is 135 ps in the CH_1 or CH_2 output port, the fall time is 295 ps in the CH_3 or CH_4 output port, and the rise time of the output optical signal is close to the loaded driving signal. Similarly, reasonably setting the driving signal status of RF_1, as shown in Table I, and loading the pulse signals at RF_{2-1}, that is, the rising and falling signals are observed at CH_1 and CH_2, the rise and fall times are 125 ps and 250 ps, respectively, as shown in Fig. 11(b). When RF_{2-2} is loaded with pulse signals, rising and falling signals are observed at CH_3 and CH_4, and the rise and fall times are 140 ps and 340 ps, respectively, as shown in Fig. 11(c). The above experimental results also show that due to the limitation of the rise time of the driving pulse signal source, the rise time of the electro-optical switch is similar to the rise time of the driving signal. Thus, the rise time of the proposed and fabricated electro-optical switch will be less than 140 ps.

TABLE III
COMPARISON WITH THE LITERATURE

Ref.	Structure of the optical-switch	Response Time	extinction ratio	Insertion Loss	Wavelength range
[6]	1×2	22 ns	17.39 dB	< 7.1 dB	
[29]	2×2	30 ns	15 dB	< 8.5 dB	85 nm
[32]	1×2		14.7 dB	11.7 dB	
[33]	1×1		35 dB	8.0 dB	12 nm
[34]	1×2		23 dB	2.5 dB	80 nm
The work	1×4	< 140ps	39.3 dB	< 7.1 dB	50 nm

Table III summarizes the comparative study of the proposed cascaded dual-output MZI optical-switch in the lithium niobate platform with some of the other techniques in the literature.

V. CONCLUSION

This paper proposes an ultrafast and high extinction ratio 1×4 electro-optic switch on the lithium niobate platform. First, the optical waveguide structure and the modulation electrode are designed and optimized by theoretical simulation. The influence of the coupling distance and coupling length of the directional coupler on the wavelength bandwidth and process tolerance have also been analyzed, and the optimized parameters of the MZI optical switch unit have been obtained. Second, the device was fabricated, and the performance of the device was tested. By applying a voltage to each electrode to complete the optical signal switching of four output ports, the insertion loss of the four ports is less than 7.1 dB, and the extinction ratio is higher than 39.3 dB. In addition, it is tested to achieve a high extinction ratio greater than 20 dB in the wavelength range of 50 nm. The half-wave voltage is less than 4.13 V, and the switching rise and fall times reach 125 ps and 250 ps, respectively. The test results show that the performance of the proposed and fabricated 1×4 high-speed electro-optic switch has the advantages of a fast response rate, high extinction ratio, and low switching voltage.

ACKNOWLEDGMENT

The authors thank Yukang Chen and Pingping Liu, graduate students of the research group, for their technical assistance with this paper.

REFERENCES

[1] Y. Zhang et al., "All-fiber nonvolatile broadband optical switch using an all-optical method," *Opt. Lett.*, vol. 47, no. 14, pp. 3604–3607, Jul. 2022.
[2] H. Zhou, Y. Zhao, X. Wang, D. Gao, J. Dong, and X. Zhang, "Self-configuring and reconfigurable silicon photonic signal processor," *ACS Photon.*, vol. 7, no. 3, pp. 792–799, Mar. 2020.

[3] A. Tayduganov et al., "Optimizing the deployment of quantum key distribution switch-based networks," *Opt. Exp.*, vol. 29, no. 16, pp. 24884–24898, Aug. 2021.

[4] R. Zhu, X. Zhou, N. Yang, L. Leng, and W. Jiang, "Towards high extinction ratio in silicon thermo-optic switches-unravelling complexity of fabrication variation," *IEEE Photon. J.*, vol. 10, no. 4, Aug. 2018, Art. no. 7905708.

[5] X. Zhao, C. Chen, S. Yuan, and X. Liu, "A robust and ultra-high extinction ratio optical switch enabled by optical diffractive network," *IEEE Photon. Technol. Lett.*, vol. 34, no. 10, pp. 549–552, May 2022.

[6] X. Zhang et al., "An optical switch based on electro-optic mode deflection in lithium niobate waveguide," *IEEE Photon. Technol. Lett.*, vol. 32, no. 20, pp. 1295–1298, Oct. 2020.

[7] Z. Pan et al., "On-chip cyclic-AWG-based 12×12 silicon wavelength routing switches with minimized port-to-port insertion loss fluctuation," *Photon. Res.*, vol. 6, no. 5, pp. 380–384, May 2018.

[8] J. Wan, W. Yuan, Y. Chen, X. Zhu, M. Guo, and P. Xu, "1×5 microfluidic optical switch using double drives," *J. Modern Opt.*, vol. 68, no. 21, pp. 1251–1258, Dec. 2021.

[9] C.-H. Tsai and J.-C. Tsai, "MEMS optical switches and interconnects," *Displays*, vol. 37, pp. 33–40, Apr. 2015.

[10] W. M. Mellette and J. E. Ford, "Scaling limits of MEMS beam-steering switches for data center networks," *J. Lightw. Technol.*, vol. 33, no. 15, pp. 3308–3318, Aug. 2015.

[11] M. Stepanovsky, "A comparative review of MEMS-Based optical cross-connects for all-optical networks from the past to the present day," *IEEE Commun. Surv. Tut.*, vol. 21, no. 3, pp. 2928–2946, thirdquarter 2019.

[12] A. J. Mercante, P. Yao, S. Shi, G. Schneider, J. Murakowski, and D. W. Prather, "110 GHz CMOS compatible thin film $LiNbO_3$ modulator on silicon," *Opt. Exp.*, vol. 24, no. 14, pp. 15590–15595, Jul. 2016.

[13] B. G. Lee, A. Biberman, N. Sherwood-Droz, C. B. Poitras, M. Lipson, and K. Bergman, "High-speed 2×2 switch for multiwavelength silicon-photonic networks-on-chip," *J. Lightw. Technol.*, vol. 27, no. 14, pp. 2900–2907, Jul. 2009.

[14] J. Liu, Q. Huang, S. Tao, C. Zeng, and J. Xia, "Low-cost hybrid integrated 4×25.78 Gb/s CWDM TOSA for 10 km transmission using DFB-LDs and an arrayed waveguide grating multiplexer," *Photon. Res.*, vol. 6, no. 11, pp. 1067–1073, Nov. 2018.

[15] M. Kudo et al., "A proposal of Mach-Zehnder mode/wavelength multi/demultiplexer based on Si/Silica hybrid PLC platform," *Opt. Commun.*, vol. 433, pp. 168–172, Feb. 2019.

[16] W. Y. Chan, K. X. Chen, H. P. Chan, B. P. Pal, and R. K. Varshney, "A flattop PLC polymer waveguide interleaver based on folded two-stage-cascaded Y-junction mach-zehnder interferometers," *Opt. Commun.*, vol. 282, no. 5, pp. 883–886, Mar. 2009.

[17] A. Bile, M. Chauvet, H. Tari, and E. Fazio, "Supervised learning of soliton X-junctions in lithium niobate films on insulator," *Opt. Lett.*, vol. 47, no. 22, pp. 5893–5896, Nov. 2022.

[18] M. Thomaschewski, V. A. Zenin, C. Wolff, and S. I. Bozhevolnyi, "Plasmonic monolithic lithium niobate directional coupler switches," *Nature Commun.*, vol. 11, no. 1, Feb. 2020, Art. no. 23154.

[19] Y. Zhang et al., "All-Optical synapse with directional coupler structure based on phase change material," *IEEE Photon. J.*, vol. 13, no. 4, Aug. 2021, Art. no. 8700106.

[20] Q. Huang, K. S. Chiang, and W. Jin, "Thermo-optically controlled vertical waveguide directional couplers for mode-selective switching," *IEEE Photon. J.*, vol. 10, no. 6, Dec. 2018, Art. no. 6602714.

[21] X. Zi, L. Wang, K. Chen, and K. S. Chiang, "Mode-Selective switch based on thermo-optic asymmetric directional coupler," *IEEE Photon. Technol. Lett.*, vol. 30, no. 7, pp. 618–621, Apr. 2018.

[22] S. - J. Chang, C. - Y. Ni, Z. Wang, and Y. - J. Chen, "A compact and low power consumption optical switch based on microrings," *IEEE Photon. Technol. Lett.*, vol. 20, no. 9-12, pp. 1021–1023, Jun. 2008.

[23] L. Chen, Q. Xu, M. G. Wood, and R. M. Reano, "Hybrid silicon and lithium niobate electro-optical ring modulator," *Optica*, vol. 1, no. 2, pp. 112–118, Aug. 2014.

[24] P. DasMahapatra, R. Stabile, A. Rohit, and K. A. Williams, "Optical crosspoint matrix using broadband resonant switches," *IEEE J. Sel. Topics Quantum Electron.*, vol. 20, no. 4, Jul./Aug. 2014, Art. no. 5900410.

[25] N. Xie, T. Hashimoto, and K. Utaka, "Very low power operation of compact MMI polymer thermooptic switch," *IEEE Photon. Technol. Lett.*, vol. 21, no. 18, pp. 1335–1337, Sep. 2009.

[26] R. B. Priti, F. Shokraneh, and O. Liboiron-Ladouceur, "Scalable 2×2 multimode switch for mode-multiplexed silicon photonics interconnects," in *Proc. Asia Commun. Photon. Conf. Exhib.*, 2018, pp. 1–3.

[27] L. Wang et al., "Polymeric waveguide MZI thermo-optic mode switch based on asymmetric directional coupler," *IEEE Photon. Technol. Lett.*, vol. 32, no. 4, pp. 200–203, Feb. 2020.

[28] N. Dupuis et al., "Design and fabrication of low-insertion-loss and low-crosstalk broadband 2×2 Mach-Zehnder silicon photonic switches," *J. Lightw. Technol.*, vol. 33, no. 17, pp. 3597–3606, Sep. 2015.

[29] H. Wang, X. Li, M. Zhang, and K. Chen, "Broadband 2×2 lithium niobate electro-optic switch based on a Mach-Zehnder interferometer with counter-tapered directional couplers," *Appl. Opt.*, vol. 56, no. 29, pp. 8164–8168, Oct. 2017.

[30] S. K. Raghuwanshi, A. Kumar, and S. Kumar, "1×4 signal router using three Mach-Zehnder interferometers," *Opt. Eng.*, vol. 52, no. 3, Mar. 2013, Art. no. 35002.

[31] C. A. Z. Khatun, "Implementation of 1×N router based on Mach-Zehnder interferometer electro-optic switch," in *Proc. IEEE Int. Conf. Innov. Sci., Eng. Technol.*, 2016, pp. 1–6.

[32] H. Jung, "An integrated photonic electric-field sensor utilizing a 1×2 YBB mach-zehnder interferometric modulator with a titanium-diffused lithium niobate waveguide and a dipole patch antenna," *Crystals*, vol. 9, no. 9, Sep. 2019, Art. no. 459.

[33] M. Zhang, K. Chen, W. Jin, and K. S. Chiang, "Electro-optic mode switch based on lithium-niobate Mach-Zehnder interferometer," *Appl. Opt.*, vol. 55, no. 16, pp. 4418–4422, Jun. 2016.

[34] S. M. Kostritskii, Y. N. Korkishko, and V. A. Fedorov, "Electro-optic 1 x 2 switch based on proton-exchanged channel waveguides in $linbO_3$," *Proc. SPIE*, vol. 9, pp. 1–7, 2015.